

Azimuthal asymmetry in cosmic-ray boosted dark matter flux

Chen Xia^{a,b}, Yan-Hao Xu^{a,b}, and Yu-Feng Zhou^{a,b,c,d}

^a*CAS key laboratory of theoretical Physics, Institute of Theoretical Physics,*

Chinese Academy of Sciences, Zhongguancun East Rd. 55, Beijing, 100190, China,

^b*School of Physics, University of Chinese Academy of Sciences, Yuquan Rd. 19, Beijing, 100049, China,*

^c*School of Fundamental Physics and Mathematical Sciences,*

Hangzhou Institute for Advanced Study, UCAS, Hangzhou, 310024, China,

^d*International Centre for Theoretical Physics Asia-Pacific (Beijing/Hangzhou), China.*

(Dated: June 24, 2022)

Light halo dark matter (DM) particles up-scattered by high-energy cosmic rays (referred to as CRDM) can be energetic and become detectable at conventional DM and neutrino experiments. We show that the CRDM flux has a novel and detectable morphological feature. Unlike most of the recently proposed boosted DM (BDM) models which predict azimuthally symmetric DM fluxes around the Galactic Center, the CRDM flux breaks the azimuthal symmetry significantly. Using cosmic-ray electron distribution in the whole Galaxy and optimized search region in the sky according to the morphology of the CRDM flux, we derive so far the most stringent constraints on the DM-electron scattering cross section from the Super-Kamiokande (SK) IV data, which improves the previous constraints from the SK-IV full-sky data by more than an order of magnitude. Based on the improved constraints, we predict that the azimuthal symmetry-breaking effect can be observed in the future Hyper-Kamiokande experiment at $\sim 3\sigma$ level.

Introduction. Although enormous astrophysical evidence suggests the existence of dark matter (DM) in the Universe, whether or not DM participates non-gravitational interactions remains to be unclear. Current underground DM direct detection (DD) experiments search for recoil signals from the possible scatterings between the halo DM particles (denoted as χ) and target nuclei or electrons within the detectors. Due to the detection threshold of the current experiments which is typically of $\mathcal{O}(\text{keV})$, DD experiments lose sensitivity rapidly towards lower halo DM mass m_χ below GeV (MeV) for DM particles couple dominantly to nucleus (electron). Several physical processes have been considered to lower the detection thresholds such as the bremsstrahlung radiation [1] and the Migdal effect [2, 3], etc.. The same scattering processes may occur in some astrophysical observables such as the cosmic microwave background [4], the gas cooling rate of dwarf galaxies [5, 6], the distribution of Milky Way satellites [7], Lyman- α forest [8], and hydrogen 21 cm radiations [9], etc., which can be used to constrain light DM particles, although the constraints are in general weaker.

Recently, it was realized that stringent constraints can be obtained from the elastic scatterings between cosmic-ray (CR) particles and DM particles [10–12]. High-energy CRs in the Galaxy can scatter off halo DM particles, which inevitably results in the energy-boost of a small fraction of halo DM particles (referred to as CRDM). The energetic light CRDM particles can scatter again off the target particles in the detector of the DD experiments, and deposit sufficient energy to cross the detection threshold. Due to the power-law feature of the observed CR nucleus energy spectrum $\sim E^{-3}$, the constraints on DM-nucleon scattering cross section are highly insensitive to the DM particle mass [13]. So far,

the constraints on the CRDM scattering cross sections have been extensively studied for various types of interactions [13–26], and searched by experiments [28–30].

The morphology of the CRDM flux is another important observable which can be probed by neutrino experiments with water Cherenkov detectors [31–33]. In these experiments, direction of the incoming DM particle can be inferred from the Cherenkov light emitted from the recoil particle. The morphological study of the DM flux is useful for background suppression, but more importantly, for distinguishing different mechanisms for boosted DM (BDM). Apart from CRDM, there exists a large class of BDM models where a boosted subdominant DM component arises from the interactions with the dominant halo DM, such as DM decay [34, 35], annihilation [36, 37], semi-annihilation [38–42], three-body annihilation [43–45], etc.. A common feature of these BDMs is that the predicted BDM flux is azimuthally symmetric around the Galactic Center (GC), as the dominant halo DM density profile is approximate spherically symmetric around the GC [46–48].

This common azimuthal symmetry is expected to be broken significantly for CRDM flux, due to the unique distribution of the CRs, which makes it possible to single out CRDM from all of the other BDM models in the future experiments. In this letter, taking the CR electron (CRE) up-scattered DM as an example, we show that CRDM breaks the azimuthal symmetry in a significant way. Using the up-to-date CR propagation model and optimized region-of-interest in the sky according to the morphology of the CRDM flux, we derive the most stringent constraints on the DM-electron scattering cross section from the Super-Kamiokande (SK) IV data. We predict that the azimuth symmetry breaking can be observed in the future Hyper-Kamiokande (HK) experiment

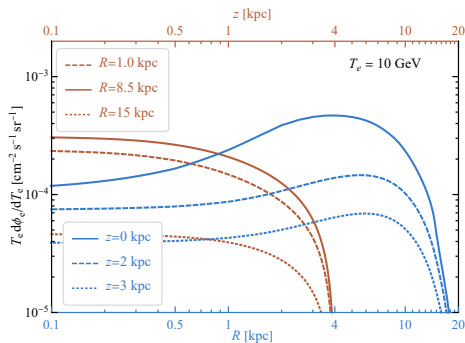


FIG. 1. The CRE intensity as a function of the cylinder distance R at different heights $z = 0, 2$ and 3 kpc (blue curves). The kinetic energy of CRE is fixed at 10 GeV. The intensity as a function of height z (upper axes) at different distances $R = 1, 8.5,$ and 15 kpc (red curves) are also shown for comparison.

at a high significance and can be easily distinguished from other BDMs.

CRDM. The distribution of the Galactic CRE intensity $d\Phi_e(\mathbf{r})/dT_e$ (number of particles emitted per unit time, area, solid angle and kinetic energy) which sources the CRDM is highly inhomogeneous. The propagation of Galactic CRE can be approximated as a diffusion process confined in a thin cylindrical diffusion halo with cylinder radius R_h and half-height z_h . The CR intensity $d\Phi_e(\mathbf{r})/dT_e$ can be obtained from solving the standard steady-state diffusion equation [49, 50]. It is generally believed that the primary sources of CREs are dominated by Supernova Remnants (SNRs). Thus the spatial distribution of the CRE source $q_e(R, z)$ is assumed to follow the standard SNR distribution $q_e(R, z) \propto (R/R_\odot)^a \exp(-bR/R_\odot - |z|/z_s)$ [51], where R and z are the cylinder coordinates, $R_\odot = 8.5$ kpc is the distance from the Earth to the GC, and $z_s \approx 0.2$ kpc is the characteristic half-height of the Galactic disk. The values of the two parameters are $a \approx 1.25$ and $b \approx 3.56$ determined from Fermi-LAT data [52, 53].

We use the numerical code `GalProp-v54` [54–58] to solve the diffusion equation, and the code `HelMod-4.2` [59] to calculate the effect of solar modulation of low energy CREs, respectively. The propagation parameters are taken from [60], which are the values tuned to best reproduce the CRE data of AMS-02 [61] and Voyager 1 [62]. In this model, the boundary of the diffusion halo is $R_h = 20$ kpc and $z_h = 4$ kpc. Other propagation parameters are discussed listed in the Supplementary Material. In Fig. 1, we show how the calculated CRE intensity $d\Phi_e(\mathbf{r})/dT_e$ changes with the distance R or height z for a typical CRE kinetic energy $T_e = 10$ GeV. The CRE flux increases with increasing R first and peaks at $R \sim 4$ kpc, then decreases rapidly towards the boundary at R_h . The variation of the intensity with z is relatively smooth for $z \lesssim 1$ kpc, but quickly

drops as z approaches z_h . This non-spherically symmetric nature of the CRE intensity is determined by both the CR distribution and the geometry of the diffusion halo, which is common to all the current CR propagation models.

We assume that the interactions between DM particles (with mass m_χ) and electrons, whether in the galaxy, the crust of the Earth, or the underground detectors, are dominated by two-body elastic scattering processes. The DM particles up-scattered by CREs should travel in straight lines in the Galaxy. The flux of CRDM at the surface of the Earth from a given direction of observation can be written as

$$\frac{d\Phi_\chi}{dT_\chi d\Omega} = \int_{\text{l.o.s}} d\ell \frac{\rho_\chi(\mathbf{r})}{m_\chi} \int_{T_e^{\min}} dT_e \frac{\sigma_{\chi e}}{T_\chi^{\max}} \frac{d\Phi_e(\mathbf{r})}{dT_e}, \quad (1)$$

where T_χ^{\max} is the maximal recoil energy of χ from the collision with an incident electron with T_e , and T_e^{\min} is the minimally required T_e to produce a recoil energy T_χ in the same collision [11]. $\sigma_{\chi e}$ is the total cross section and $\rho_\chi(\mathbf{r})$ is the DM density distribution function. We have assumed that the scattering is isotropic in the DM-electron center-of-mass frame. The integration of the CRDM flux generated at different positions is performed along the line-of-sight (l.o.s) of observation. It is obvious from Eq. (1) that the CRDM flux has an additional dependence on the CRE distribution $d\Phi_e(\mathbf{r})/dT_e$.

Morphology of boosted DM. The morphology of DM flux is important for detection and distinguishing different mechanisms of boosted DM. For instance, DM accelerated by the Sun [63–66], supernova [67] and blazars [68] should be observed as point-like sources. The DM flux generated from inelastic scatterings between CRs and the atmosphere of the Earth [69] are expected to be isotropic. Note that there exists a large class of boosted DM models (BDM) where a subdominant energetic DM component is produced from the interaction with the dominant halo DM. For this type of models, the anisotropy in the boosted DM flux *solely* originates from the halo DM density distribution and the corresponding DM flux can be generally written as

$$\frac{d\Phi_\chi^{\text{BDM}}}{dT_\chi d\Omega} \propto \int_{\text{l.o.s}} d\ell \rho_\chi(\mathbf{r})^n, \quad (2)$$

where n is a model-dependent integer. Some examples of these models include: *i*) *DM decay*. In this type of model, there are at least two DM components χ_A and χ_B . The boosted DM particle χ_B is produced through the decay of the dominant heavier component χ_A through $\chi_A \rightarrow \chi_B \bar{\chi}_B$, which corresponds to the case of $n = 1$ [34, 35]. The model with DM produced from the evaporation of primordial black holes also falls into this type [70–72]. *ii*) *DM two-body annihilation*. The boosted DM particle χ_B arises from the annihilation of the dominant component χ_A through the process $\chi_A \bar{\chi}_A \rightarrow \chi_B \bar{\chi}_B$

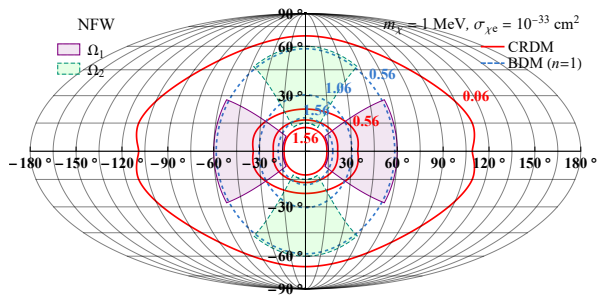


FIG. 2. Contours of CRDM flux (red solid) $d\Phi_\chi/d\Omega$ (in units of $10^{-5}\text{cm}^{-2}\text{s}^{-1}\text{sr}^{-1}$) with energy $T_e > 0.1$ GeV for a typical case of $\sigma_{\chi e} = 1 \times 10^{-33}\text{cm}^2$ and $m_\chi = 1$ MeV. The contours of BDM with $n = 1$ (blue dashed) which is azimuthally symmetric is also shown for comparison. The optimized regions Ω_1 (magenta) and Ω_2 (green) for calculating the CRDM azimuthal asymmetry A_R are also shown. The NFW [46] DM density profile is assumed.

which corresponds to $n = 2$ [36, 37]. In some semi-annihilation models, the process of $\chi_A\bar{\chi}_A \rightarrow \chi_B\phi$ with ϕ being any other states also belongs to this type [38–42]. *iii) DM three-body annihilation* $3 \rightarrow 2$. In this scenario, three DM particles collide and produce two light DM particles $\chi_A\chi_A\chi_A \rightarrow \chi_B\bar{\chi}_B$ which corresponds to the case of $n = 3$ [43–45]. In addition, the model of boosted DM from the CR-atmosphere scattering produces an isotropic flux which falls into the trivial case of $n = 0$ [69]. Since most of the commonly adopted halo DM density $\rho(\mathbf{r})$ is spherically symmetric, i.e. $\rho(\mathbf{r}) = \rho(r)$ [46–48], the resulting boosted DM flux from all of the above mentioned models will be azimuthally symmetric around the GC.

However, the morphology of the CRDM flux is quite different. As shown in Eq. (1), the CRDM flux has an additional dependence on the CRE distribution which is not spherically symmetric. Consequently, the azimuthal symmetry is expected to be broken in CRDM flux. We calculate the CRDM flux based on our previous work [13, 25]. In Fig. 2, we show the contours of CRDM flux with energy above 0.1 GeV in the full sky for a reference $m_\chi = 1$ MeV and $\sigma_{\chi e} = 10^{-33}\text{cm}^2$, and the flux of BDM with $n = 1$. The BDM flux is normalized in such a way that the total flux within polar angle $\theta \leq 5^\circ$ is the same as that from CRDM. The DM profile is set to NFW [46] with a local DM density $\rho_0 = 0.42\text{GeV}\cdot\text{cm}^{-3}$ and characteristic radius $r_s = 20$ kpc. It can be clearly seen that compared with the BDM, the CRDM flux decreases faster towards higher galactic altitude, which explicitly breaks the azimuth symmetry.

Azimuthal asymmetry. The azimuthal symmetry breaking effect can be quantified using the standard spherical harmonic expansion of the CRDM flux $\frac{d\Phi_\chi}{d\Omega} = \sum_{l,m} a_{l,m} Y_{l,m}(\theta, \varphi)$, where $Y_{l,m}(\theta, \varphi)$ are the spherical harmonic function with integer indices l and m . θ and φ are the polar and azimuth angle, respectively. For any function with azimuth symmetry such as the BDM flux,

the φ dependence disappear. Consequently, $a_{l,m} = 0$ for all $m \neq 0$. For CRDM, the azimuthal symmetry breaking results in non-vanishing $a_{l,m}$ for m being nonzero even numbers. The coefficients with odd-numbered m are still zero as the CR source term $q_e(R, z)$ is symmetric under $z \rightarrow -z$. In Tab. I, we show a selection of the extracted

	$\tilde{a}_{1,0}$	$\tilde{a}_{2,0}$	$\tilde{a}_{3,0}$	$\tilde{a}_{2,2}$	$\tilde{a}_{3,2}$	$\tilde{a}_{4,2}$
CRDM	1.00	0.90	0.76	0.12	0.12	0.11
BDM ($n = 2$)	1.28	1.33	1.32	0	0	0
BDM ($n = 1$)	0.63	0.37	0.24	0	0	0

TAB. I. A selection of extracted normalized coefficients $\tilde{a}_{l,m}$ of the spherical harmonic functions for three type of DM models.

coefficients $\tilde{a}_{l,m} = |a_{l,m}|/|a_{0,0}|$ normalized to the leading term $|a_{0,0}|$ from the distribution of the CRDM flux and the BDM flux with $n = 1, 2$, using the numerical code **Healpix-3.8** [73]. These coefficients are independent of the interaction cross sections or decay lifetime. The table shows that only the CRDM has the nonvanishing coefficients $\tilde{a}_{l,2}$, and the typical size reaches $\sim 10\%$ relative to the leading dipole coefficients $\tilde{a}_{1,0}$. The coefficients are insensitive to the choice of DM profiles, The difference is found to be within 10% for the Einasto profile [47]. A more complete list of the coefficients are listed in the Supplementary Material.

Alternatively, the azimuth symmetry breaking of the CRDM flux can be quantified by the difference in event number in two equal-area regions $\Omega_{1,2}$ in the sky which are related by a rotation around the GC. We consider the following asymmetric parameter

$$A_R = \frac{N(\Omega_1) - N(\Omega_2)}{N(\Omega_1) + N(\Omega_2)}, \quad (3)$$

where $N(\Omega_i)$ is the number of predicted events in the region Ω_i under consideration. The number of events can be written as the sum of signal and background, i.e., $N(\Omega_i) = S(\Omega_i) + B(\Omega_i)$. For a given background event rate, it is necessary to optimize the shapes of Ω_i to maximize the statistical significant of the asymmetry A_R . We find that for the background-dominant case, the best regions for Ω_1 are two annular sectors with inner (outer) angular radius $\theta_{1(2)} = 15$ (60) $^\circ$ and open angle $\varphi = 65^\circ$ which are centered along the Galactic plane. The regions of Ω_2 are obtained through a 90° rotation of Ω_1 , which are illustrated in Fig. 2. For a typical cross section of $\sigma_{\chi e} = 10^{-33}\text{cm}^2$ at $m_\chi = 1$ MeV, the contribution from CRDM alone to the asymmetry reaches $A_R = 0.34$ in this region. Of course, A_R should decrease significantly after the background is taken into account. The value of A_R is insensitive to the choice of DM profile as the inner region close to the GC is excluded.

Improved SK-IV limits. Before arriving at the underground detectors, CRDM particles may lose energy

due to the same elastic scattering off the electrons inside the crust of the Earth. For calculating the effect of Earth attenuation, we use the numerical simulation code `DarkProp` [74] developed in our previous work for the Earth attenuation of CRDM [25]. After passing through the Earth, the CRDM particles can scatter again off the electrons in the underground detector, which can be detected by the Cherenkov light emitted by the recoil electron. Since the CRDM particle under consideration is quite energetic, we assume that the electron before the scattering is a free electron at rest, and the recoil electron after the scattering closely follows the direction of the incoming CRDM particle. The differential event rate per unit target mass in a solid angle $\Delta\Omega$ of observation is given by

$$\frac{d\bar{\Gamma}}{dT_e} = \mathcal{N}_e \int_{\Delta\Omega} d\Omega \int_{T_\chi^{\min}}^{T_\chi^{\max}} dT_\chi \frac{\sigma_{\chi e}}{T_e^{\max}} \frac{d\Phi_\chi}{dT_\chi d\Omega}, \quad (4)$$

where T_e^{\max} is the maximal energy that can be produced by the CRDM particle with incident energy T_χ , and T_χ^{\min} is the minimal energy required for the CRDM particle to produce a recoil energy T_e . \mathcal{N}_e is the number of electrons per unit target mass. The SK experiment is located at ~ 1 km underground, which uses large water Cherenkov detectors with 22.5 kt fiducial mass and a good angular resolution [75]. For water Cherenkov detectors $\mathcal{N}_e \approx 3.3 \times 10^{26} \text{ kg}^{-1}$. The SK collaboration has performed a search for BDMs based on the SK-IV data with an exposure of 161.9 kt · yr. The SK results have been translated into constraints on the CRE boosted DM previously in [12]. This pioneering analysis, however, depended on an unconstrained parameter of CRE cylinder height h which is assumed to be ~ 1 kpc. Furthermore, an uniform distribution of CR in the whole Galaxy was assumed, which prevent accurate analysis of the event angular distribution.

We perform a significantly improved analysis by using the realistic Galactic CRE distribution and optimized search region, which allows for fully exploring the information provided by the SK-IV data. In the search for BDMs, the SK collaboration provided limits on the e -like events in different cones around the GC with the polar angle θ ranging from 5° to 40° in steps of 5° . We first determine the optimized cone region which can maximize the ratio S/\sqrt{B} for CRDM. We use an isotropic background event rate of $1.96 \text{ kt}^{-1} \text{ yr}^{-1} \text{ sr}^{-1}$ from the SK MC simulation [76], and calculate the signal in the first energy bin $0.1 - 1.33$ GeV with detection efficiency included. The search result shows that the region within $\theta \leq 25^\circ$ gives the highest signal significance. Through directly translate the limits from the SK analysis in this sky region the same energy bin, we obtain so far the most stringent limits which are shown in Fig. 3. In particular, we find that the limit reaches $\sigma_{\chi e} \leq 2.4 \times 10^{-33} \text{ cm}^2$ at $m_\chi = 1$ MeV. These new limits improved the previous

constraints in [12] by a factor of ~ 17 , in which a factor of two of improvement comes from the optimized cone size. The results are also stronger than that derived from the SK-I low energy data for relic neutrino search [14].

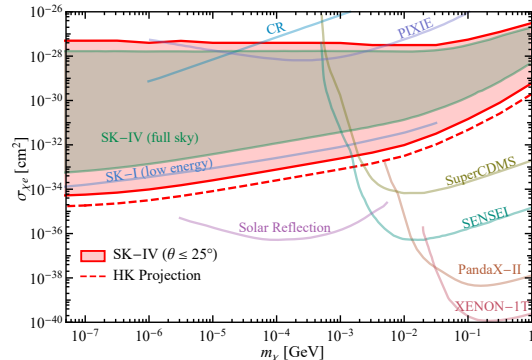


FIG. 3. Exclusion regions in $(m_\chi, \sigma_{\chi e})$ plane at 90% C.L. derived from SK-IV data (red solid) with events inside the cone with $\theta \leq 25^\circ$. The exclusion regions derived from the full-sky SK-IV data [12], and that derived from SK-I low energy data [14] are also shown. A selection of other constraints such as that from PIXIE [77], XENON-1T [78], PandaX-II [79], SENSEI [80], SuperCDMS [81], cosmic ray [10] and solar reflection [64] are shown for comparison. The projected constraints from the future HK experiment (red dashed) are shown.

Projections for HK. Using the updated constraints, we estimate the asymmetry A_R in the current and the future experiments in the same energy bin. We find that for the maximally allowed cross section $\sigma_{\chi e} = 2.4 \times 10^{-33} \text{ cm}^2$ at $m_\chi = 1$ MeV, the predicted asymmetry at SK is $A_R^{\text{SK}} = 0.017 \pm 0.036$, which is not statistically significant due to the large background of SK. Note that the statistical uncertainty will decrease with increasing exposure, it is possible to observe a more significant signal in the future experiments with larger exposures. In Fig. 4, we show how the significance of A_R changes with the increasing exposure. As an example, we consider the future water Cherenkov detector of Hyper-Kamiokande (HK) which is designed to have a total fiducial volume 16.8 times of the SK [82]. For simplicity, we assume that the background event rate of HK is the same as that of SK so that the major difference is related to the exposure. The HK is designed to run for at least 20 years with the total exposure reaching $\sim 7.6 \text{ Mt} \cdot \text{yr}$ [83]. For the 20 years of HK data taking, the asymmetry is projected to be

$$A_R^{\text{HK}} = (1.73 \pm 0.55) \times 10^{-2}, \quad (5)$$

namely, A_R can be more than 3σ above zero. All the BDMs described in Eq. (2) predict a vanishing A_R , so the uncertainties for BDMs are merely from the background, as shown in Fig. 4 for the case of $n = 1$. We find that for HK the two class of scenarios can be distinguished

at $\sim 2\sigma$ level. If no positive signals are observed in the future HK, more stringent constraints on CRDM can be obtained. We assume that the backgrounds and signals scale with the exposure, and use the maximal-likelihood method to derive the constraints in the searching cone of $\theta \leq 25^\circ$, as we did for the SK-IV data. The results shown in Fig. 3 suggest that the current best constraints can be improved by around a factor of three.

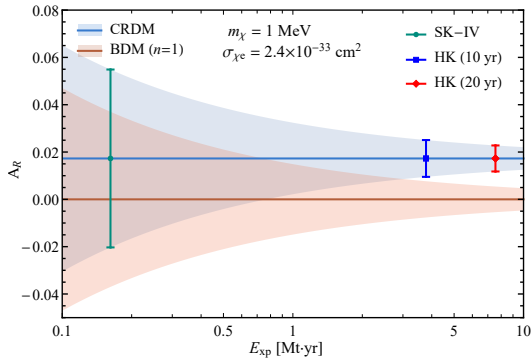


FIG. 4. Azimuthal symmetry breaking parameter A_R and its uncertainty as a function of the exposure, for DM mass $m_\chi = 1$ MeV and cross section $\sigma_{\chi e} = 2.4 \times 10^{-33}$ cm². The typical exposures for 0.16 Mt·yr (SK-IV), 3.8 Mt·yr (10 years of HK) and 7.6 Mt·yr (20 years of HK) are marked as green, blue and red, respectively. The results from BDM with $n = 1$ are also shown.

Conclusions. We have studied the morphological feature of the CRDM, which can be used not only to improve the constraints on the DM-electron scattering cross section but also distinguish it from a large class of boosted DM models in the future experiments. We have focused the CRE boosted DM. It is straight forward to extend the analysis to DM-nucleon scattering process, as it has been shown that the identification of proton track is possible at SK [20, 84].

This work is supported in part by the National Key R&D Program of China No. 2017YFA0402204, the National Natural Science Foundation of China (NSFC) No. 11825506, No. 11821505, and No. 12047503.

[1] C. Kouvaris and J. Pradler, *Phys. Rev. Lett.* **118**, 031803 (2017), arXiv:1607.01789 [hep-ph].
 [2] M. Ibe, W. Nakano, Y. Shoji, and K. Suzuki, *JHEP* **03**, 194 (2018), arXiv:1707.07258 [hep-ph].
 [3] M. J. Dolan, F. Kahlhoefer, and C. McCabe, *Phys. Rev. Lett.* **121**, 101801 (2018), arXiv:1711.09906 [hep-ph].
 [4] V. Gluscevic and K. K. Boddy, *Phys. Rev. Lett.* **121**, 081301 (2018), arXiv:1712.07133 [astro-ph.CO].
 [5] D. Wadekar and G. R. Farrar, *Phys. Rev. D* **103**, 123028 (2021), arXiv:1903.12190 [hep-ph].
 [6] A. Bhoonah, J. Bramante, F. Elahi, and S. Schon, *Phys.*

Rev. Lett. **121**, 131101 (2018), arXiv:1806.06857 [hep-ph].
 [7] E. O. Nadler, V. Gluscevic, K. K. Boddy, and R. H. Wechsler, *Astrophys. J. Lett.* **878**, 32 (2019), [Erratum: *Astrophys.J.Lett.* 897, L46 (2020), Erratum: *Astrophys.J.* 897, L46 (2020)], arXiv:1904.10000 [astro-ph.CO].
 [8] R. Murgia, V. Iršič, and M. Viel, *Phys. Rev. D* **98**, 083540 (2018), arXiv:1806.08371 [astro-ph.CO].
 [9] T. R. Slatyer and C.-L. Wu, *Phys. Rev. D* **98**, 023013 (2018), arXiv:1803.09734 [astro-ph.CO].
 [10] C. V. Cappiello, K. C. Y. Ng, and J. F. Beacom, *Phys. Rev. D* **99**, 063004 (2019), arXiv:1810.07705 [hep-ph].
 [11] T. Bringmann and M. Pospelov, *Phys. Rev. Lett.* **122**, 171801 (2019), arXiv:1810.10543 [hep-ph].
 [12] Y. Ema, F. Sala, and R. Sato, *Phys. Rev. Lett.* **122**, 181802 (2019), arXiv:1811.00520 [hep-ph].
 [13] C. Xia, Y.-H. Xu, and Y.-F. Zhou, *Nucl. Phys. B* **969**, 115470 (2021), arXiv:2009.00353 [hep-ph].
 [14] C. V. Cappiello and J. F. Beacom, *Phys. Rev. D* **100**, 103011 (2019), [Erratum: *Phys.Rev.D* 104, 069901 (2021)], arXiv:1906.11283 [hep-ph].
 [15] G. Krnjaic and S. D. McDermott, *Phys. Rev. D* **101**, 123022 (2020), arXiv:1908.00007 [hep-ph].
 [16] J. B. Dent, B. Dutta, J. L. Newstead, and I. M. Shoemaker, *Phys. Rev. D* **101**, 116007 (2020), arXiv:1907.03782 [hep-ph].
 [17] K. Bondarenko, A. Boyarsky, T. Bringmann, M. Hufnagel, K. Schmidt-Hoberg, and A. Sokolenko, *JHEP* **03**, 118 (2020), arXiv:1909.08632 [hep-ph].
 [18] W. Wang, L. Wu, J. M. Yang, H. Zhou, and B. Zhu, *JHEP* **12**, 072 (2020), [Erratum: *JHEP* 02, 052 (2021)], arXiv:1912.09904 [hep-ph].
 [19] J. B. Dent, B. Dutta, J. L. Newstead, I. M. Shoemaker, and N. T. Arellano, *Phys. Rev. D* **103**, 095015 (2021), arXiv:2010.09749 [hep-ph].
 [20] Y. Ema, F. Sala, and R. Sato, *SciPost Phys.* **10**, 072 (2021), arXiv:2011.01939 [hep-ph].
 [21] G. Guo, Y.-L. S. Tsai, M.-R. Wu, and Q. Yuan, *Phys. Rev. D* **102**, 103004 (2020), arXiv:2008.12137 [astro-ph.HE].
 [22] G. Guo, Y.-L. S. Tsai, and M.-R. Wu, *JCAP* **10**, 049 (2020), arXiv:2004.03161 [astro-ph.HE].
 [23] W. Wang, L. Wu, W.-N. Yang, and B. Zhu, (2021), arXiv:2111.04000 [hep-ph].
 [24] S.-F. Ge, J. Liu, Q. Yuan, and N. Zhou, *Phys. Rev. Lett.* **126**, 091804 (2021), arXiv:2005.09480 [hep-ph].
 [25] C. Xia, Y.-H. Xu, and Y.-F. Zhou, *JCAP* **02**, 028 (2022), arXiv:2111.05559 [hep-ph].
 [26] N. F. Bell, J. B. Dent, B. Dutta, S. Ghosh, J. Kumar, J. L. Newstead, and I. M. Shoemaker, *Phys. Rev. D* **104**, 076020 (2021), arXiv:2108.00583 [hep-ph].
 [27] A. Granelli, P. Ullio, and J.-W. Wang, (2022), arXiv:2202.07598 [astro-ph.HE].
 [28] M. Andriamirado *et al.* (PROSPECT, (PROSPECT Collaboration)*), *Phys. Rev. D* **104**, 012009 (2021), arXiv:2104.11219 [hep-ex].
 [29] X. Cui *et al.* (PandaX-II), *Phys. Rev. Lett.* **128**, 171801 (2022), arXiv:2112.08957 [hep-ex].
 [30] R. Xu *et al.* (CDEX), (2022), arXiv:2201.01704 [hep-ex].
 [31] K. Abe *et al.* (Super-Kamiokande), *Phys. Rev. D* **94**, 052010 (2016), arXiv:1606.07538 [hep-ex].
 [32] B. Aharmim *et al.* (SNO), *Phys. Rev. C* **81**, 055504 (2010), arXiv:0910.2984 [nucl-ex].

- [33] M. Anderson *et al.* (SNO+), *Phys. Rev. D* **99**, 012012 (2019), [arXiv:1812.03355 \[hep-ex\]](#).
- [34] J. Kopp, J. Liu, and X.-P. Wang, *JHEP* **04**, 105 (2015), [arXiv:1503.02669 \[hep-ph\]](#).
- [35] A. Bhattacharya, R. Gandhi, A. Gupta, and S. Mukhopadhyay, *JCAP* **05**, 002 (2017), [arXiv:1612.02834 \[hep-ph\]](#).
- [36] K. Agashe, Y. Cui, L. Necib, and J. Thaler, *JCAP* **10**, 062 (2014), [arXiv:1405.7370 \[hep-ph\]](#).
- [37] G. Belanger and J.-C. Park, *JCAP* **03**, 038 (2012), [arXiv:1112.4491 \[hep-ph\]](#).
- [38] F. D'Eramo and J. Thaler, *JHEP* **06**, 109 (2010), [arXiv:1003.5912 \[hep-ph\]](#).
- [39] T. Hambye, *JHEP* **01**, 028 (2009), [arXiv:0811.0172 \[hep-ph\]](#).
- [40] T. Hambye and M. H. G. Tytgat, *Phys. Lett. B* **683**, 39 (2010), [arXiv:0907.1007 \[hep-ph\]](#).
- [41] C. Arina, T. Hambye, A. Ibarra, and C. Weniger, *JCAP* **03**, 024 (2010), [arXiv:0912.4496 \[hep-ph\]](#).
- [42] G. Belanger, K. Kannike, A. Pukhov, and M. Raidal, *JCAP* **04**, 010 (2012), [arXiv:1202.2962 \[hep-ph\]](#).
- [43] E. D. Carlson, M. E. Machacek, and L. J. Hall, *Astrophys. J.* **398**, 43 (1992).
- [44] A. A. de Laix, R. J. Scherrer, and R. K. Schaefer, *Astrophys. J.* **452**, 495 (1995), [arXiv:astro-ph/9502087](#).
- [45] Y. Hochberg, E. Kuflik, T. Volansky, and J. G. Wacker, *Phys. Rev. Lett.* **113**, 171301 (2014), [arXiv:1402.5143 \[hep-ph\]](#).
- [46] J. F. Navarro, C. S. Frenk, and S. D. M. White, *Astrophys. J.* **462**, 563 (1996), [arXiv:astro-ph/9508025](#).
- [47] J. Einasto (2009) [arXiv:0901.0632 \[astro-ph.CO\]](#).
- [48] J. N. Bahcall and R. M. Soneira, *Astrophys. J. Suppl.* **44**, 73 (1980).
- [49] V. S. Berezinsky, S. V. Bulanov, V. A. Dogiel, and V. S. Ptuskin, *Astrophysics of cosmic rays*, edited by V. L. Ginzburg (1990).
- [50] A. W. Strong, I. V. Moskalenko, and V. S. Ptuskin, *Ann. Rev. Nucl. Part. Sci.* **57**, 285 (2007), [arXiv:astro-ph/0701517](#).
- [51] G. Case and D. Bhattacharya, *Astron. Astrophys. Suppl.* **120**, 437 (1996).
- [52] R. Trotta, G. Jóhannesson, I. V. Moskalenko, T. A. Porter, R. R. d. Austri, and A. W. Strong, *Astrophys. J.* **729**, 106 (2011), [arXiv:1011.0037 \[astro-ph.HE\]](#).
- [53] L. Tibaldo and I. A. Grenier (Fermi-LAT), (2009), [arXiv:0907.0312 \[astro-ph.HE\]](#).
- [54] A. W. Strong and I. V. Moskalenko, *Astrophys. J.* **509**, 212 (1998), [arXiv:astro-ph/9807150](#).
- [55] I. V. Moskalenko, A. W. Strong, J. F. Ormes, and M. S. Potgieter, *Astrophys. J.* **565**, 280 (2002), [arXiv:astro-ph/0106567](#).
- [56] A. W. Strong and I. V. Moskalenko, *Adv. Space Res.* **27**, 717 (2001), [arXiv:astro-ph/0101068](#).
- [57] I. V. Moskalenko, A. W. Strong, S. G. Mashnik, and J. F. Ormes, *Astrophys. J.* **586**, 1050 (2003), [arXiv:astro-ph/0210480](#).
- [58] V. S. Ptuskin, I. V. Moskalenko, F. C. Jones, A. W. Strong, and V. N. Zirakashvili, *Astrophys. J.* **642**, 902 (2006), [arXiv:astro-ph/0510335](#).
- [59] M. J. Boschini *et al.*, *Astrophys. J.* **840**, 115 (2017), [arXiv:1704.06337 \[astro-ph.HE\]](#).
- [60] M. J. Boschini *et al.*, *Astrophys. J.* **854**, 94 (2018), [arXiv:1801.04059 \[astro-ph.HE\]](#).
- [61] M. Aguilar *et al.* (AMS), *Phys. Rev. Lett.* **113**, 121102 (2014).
- [62] A. C. Cummings, E. C. Stone, B. C. Heikkila, N. Lal, W. R. Webber, G. Jóhannesson, I. V. Moskalenko, E. Orlando, and T. A. Porter, *Astrophys. J.* **831**, 18 (2016).
- [63] C. Kouvaris, *Phys. Rev. D* **92**, 075001 (2015), [arXiv:1506.04316 \[hep-ph\]](#).
- [64] H. An, M. Pospelov, J. Pradler, and A. Ritz, *Phys. Rev. Lett.* **120**, 141801 (2018), [Erratum: *Phys.Rev.Lett.* **121**, 259903 (2018)], [arXiv:1708.03642 \[hep-ph\]](#).
- [65] Y. Zhang, *PTEP* **2022**, 013B05 (2022), [arXiv:2001.00948 \[hep-ph\]](#).
- [66] J. H. Chang, D. E. Kaplan, S. Rajendran, H. Ramani, and E. H. Tanin, (2022), [arXiv:2205.11527 \[hep-ph\]](#).
- [67] Y.-H. Lin, W.-H. Wu, M.-R. Wu, and H. T.-K. Wong, (2022), [arXiv:2206.06864 \[hep-ph\]](#).
- [68] A. Granelli, P. Ullio, and J.-W. Wang, (2022), [arXiv:2202.07598 \[astro-ph.HE\]](#).
- [69] J. Alvey, M. Campos, M. Fairbairn, and T. You, *Phys. Rev. Lett.* **123**, 261802 (2019), [arXiv:1905.05776 \[hep-ph\]](#).
- [70] R. Calabrese, M. Chianese, D. F. G. Fiorillo, and N. Saviano, *Phys. Rev. D* **105**, L021302 (2022), [arXiv:2107.13001 \[hep-ph\]](#).
- [71] W. Chao, T. Li, and J. Liao, (2021), [arXiv:2108.05608 \[hep-ph\]](#).
- [72] R. Calabrese, M. Chianese, D. F. G. Fiorillo, and N. Saviano, *Phys. Rev. D* **105**, 103024 (2022), [arXiv:2203.17093 \[hep-ph\]](#).
- [73] K. M. Górski, E. Hivon, A. J. Banday, B. D. Wandelt, F. K. Hansen, M. Reinecke, and M. Bartelman, *Astrophys. J.* **622**, 759 (2005), [arXiv:astro-ph/0409513](#).
- [74] C. Xia, "DarkProp-v0.1," <http://yfzhou.itp.ac.cn/darkprop> (2022).
- [75] Y. Fukuda *et al.* (Super-Kamiokande), *Nucl. Instrum. Meth. A* **501**, 418 (2003).
- [76] C. Kachulis *et al.* (Super-Kamiokande), *Phys. Rev. Lett.* **120**, 221301 (2018), [arXiv:1711.05278 \[hep-ex\]](#).
- [77] Y. Ali-Haïmoud, J. Chluba, and M. Kamionkowski, *Phys. Rev. Lett.* **115**, 071304 (2015), [arXiv:1506.04745 \[astro-ph.CO\]](#).
- [78] E. Aprile *et al.* (XENON), *Phys. Rev. Lett.* **123**, 251801 (2019), [arXiv:1907.11485 \[hep-ex\]](#).
- [79] C. Cheng *et al.* (PandaX-II), *Phys. Rev. Lett.* **126**, 211803 (2021), [arXiv:2101.07479 \[hep-ex\]](#).
- [80] L. Barak *et al.* (SENSEI), *Phys. Rev. Lett.* **125**, 171802 (2020), [arXiv:2004.11378 \[astro-ph.CO\]](#).
- [81] R. Agnese *et al.* (SuperCDMS), *Phys. Rev. Lett.* **121**, 051301 (2018), [Erratum: *Phys.Rev.Lett.* **122**, 069901 (2019)], [arXiv:1804.10697 \[hep-ex\]](#).
- [82] K. Abe *et al.* (Hyper-Kamiokande), *PTEP* **2018**, 063C01 (2018), [arXiv:1611.06118 \[hep-ex\]](#).
- [83] J. Bian *et al.* (Hyper-Kamiokande), in *2022 Snowmass Summer Study*, 2203.02029.
- [84] M. Fechner *et al.* (Super-Kamiokande), *Phys. Rev. D* **79**, 112010 (2009), [arXiv:0901.1645 \[hep-ex\]](#).
- [85] G. F. Krymskii, *Soviet Physics Doklady* **22**, 327 (1977).
- [86] R. D. Blandford and J. P. Ostriker, *Astrophys. J. Lett.* **221**, L29 (1978).
- [87] A. R. Bell, *Mon. Not. Roy. Astron. Soc.* **182**, 147 (1978).
- [88] A. R. Bell, *Mon. Not. Roy. Astron. Soc.* **182**, 443 (1978).
- [89] G. Ambrosi *et al.* (DAMPE), *Nature* **552**, 63 (2017), [arXiv:1711.10981 \[astro-ph.HE\]](#).
- [90] D. Kerszberg, M. Kraus, D. Kolitzus, K. Egberts, S. Funk, J. Lenain, O. Reimer, and P. Vincent, in *Inter-*

national Cosmic Ray Conference,[CRI215] (2017).

(Supplementary Material)
Azimuthal asymmetry in cosmic-ray boosted dark matter flux

Chen Xia, Yan-Hao Xu, and Yu-Feng Zhou

CR electrons in the Galaxy

In this section, we give a brief overview of the CR propagation in the Galaxy and the values of related parameters. The diffusion of CR charged particles through the Galaxy can be approximated by a diffusion model in which the diffusion halo is parameterized by a cylinder with radius $R_h \simeq 20$ kpc and half-height $z_h = 1 \sim 10$ kpc. The diffusion equation for the CRs reads [49, 50]

$$\frac{\partial \psi}{\partial t} = \nabla \cdot (D_{xx} \nabla \psi - \mathbf{V}_c \psi) + \frac{\partial}{\partial p} p^2 D_{pp} \frac{\partial}{\partial p} \frac{1}{p^2} \psi - \frac{\partial}{\partial p} \left[\frac{dp}{dt} \psi - \frac{p}{3} (\nabla \cdot \mathbf{V}_c) \psi \right] - \frac{1}{\tau_f} \psi - \frac{1}{\tau_r} \psi + q(\mathbf{r}, p), \quad (\text{S-1})$$

where $\psi(\mathbf{r}, p, t)$ is the CR number density per unit momentum. In the above diffusion equation, D_{xx} is the spatial diffusion term which is parameterized as $D_{xx} = D_0 \beta^\eta (\rho/\rho_0)^\delta$ where $\rho = p/Ze$ is the rigidity of CR particles with electric charge Ze , ρ_0 is a reference scale, δ is the spectral power index, D_0 is a normalization constant, $\beta = v/c$ is the velocity of CR particles, and $\eta \approx 0.7$. The re-acceleration effect is described as diffusion in momentum space and is determined by the coefficient D_{pp} . The value of D_{pp} is related to D_{xx} as $D_{pp} D_{xx} = 4V_a^2 p^2 / (3\delta(4 - \delta^2)(4 - \delta))$ with V_a the Alfvén velocity of disturbances in the hydrodynamical plasma [49]. \mathbf{V}_c is the convection velocity which is assumed linearly increases with the distance z from the galactic plane with the gradient dV_c/dz . The quantity dp/dt stands for the momentum loss rate. The time scales for fragmentation and radioactive decay for CR nuclei are described by τ_f and τ_r respectively. Finally, $q(\mathbf{r}, p)$ is the source term. The spatial boundary conditions in the cylinder coordinates (R, z) are set by assuming that free particles escape beyond the halo, i.e., $\psi(R_h, z, p) = \psi(R, \pm z_h, p) = 0$. The steady-state solution can be obtained by setting $\partial \psi / \partial t = 0$.

It is generally believed that the major source of cosmic-ray electrons (CREs) is the Supernova Remnants (SNRs). The interstellar Charged particles can gain very high energy from non-relativistic diffusive shock wave through the Fermi acceleration mechanism [85–88]. The injection of the primary CR particles from the SNRs can be considered as a stable continuous source since the supernova explosion rate in the Galaxy is around three per century. The source term of the primary electrons from the SNRs can be parametrized as

$$q_{\text{prim}}(\mathbf{r}, t, p) \propto q(R, z) f(p), \quad (\text{S-2})$$

where $q(R, z)$ is the spatial distribution in the cylinder coordinate system with center at the Galactic Center (GC) and $f(p)$ is the energy-dependent part of the source term. The spatial distribution of primary source is assumed to follow the standard SNR distribution [51]

$$q(R, z) = \left(\frac{R}{R_\odot} \right)^a \exp \left(-b \frac{R - R_\odot}{R_\odot} \right) \exp \left(-\frac{|z|}{z_s} \right), \quad (\text{S-3})$$

where $R_\odot = 8.5$ kpc is the distance from the Earth to the GC. The parameters $a \approx 1.25$ and $b \approx 3.56$ are obtained by fitting Fermi-LAT γ -ray gradient [52, 53]. $z_s \approx 0.2$ kpc is the characteristic height of the Galactic disk. For CREs the energy-dependent part is assumed to have a broken power law behaviour in rigidity

$$f_e(\rho) = \begin{cases} \left(\frac{\rho}{\rho_0} \right)^{-\gamma_0} & \rho \leq \rho_0, \\ \left(\frac{\rho}{\rho_0} \right)^{-\gamma_1} & \rho_0 < \rho \leq \rho_1, \\ \left(\frac{\rho_1}{\rho_0} \right)^{-\gamma_1} \left(\frac{\rho}{\rho_1} \right)^{-\gamma_2} & \rho_1 < \rho \leq \rho_2, \\ \left(\frac{\rho_1}{\rho_0} \right)^{-\gamma_1} \left(\frac{\rho_2}{\rho_1} \right)^{-\gamma_2} \left(\frac{\rho}{\rho_2} \right)^{-\gamma_3} & \rho \geq \rho_2. \end{cases} \quad (\text{S-4})$$

In this work, we use the code `GalProp-v54` [54–58] to numerically solve the CR diffusion equation with given source distributions and boundary conditions. We adopt the propagation parameters reported by `HelMod` group [60] summarized in Tab. S-1, which are the best values tuned to the electrons data from AMS-02 [61]. The remaining

Z_h [kpc]	D_0 [10^{28} $\text{cm}^2 \text{s}^{-1}$]	δ	V_a [km s^{-1}]	dV_c/dz [$\text{km s}^{-1} \text{kpc}^{-1}$]
4.0	4.3	0.405	31	9.8
ρ_0 [GV]	ρ_1 [GV]	ρ_2 [GV]	γ_0 / γ_1	γ_2 / γ_3
0.19	6	95	2.57/1.40	2.80/2.40

TAB. S-1. Best fit values of propagation parameters and source parameters from Ref. [60].

terms including energy-loss term dp/dt , the time scale of fragmentation τ_f and radioactive decay τ_r are set to the `GalProp` default values. When CR particles enter the solar system, the flux of CR particles is affected by the solar wind and the heliospheric magnetic field, which mainly affects the CR flux in the low-energy region. We use the code `HelMod-4.2` [59] to calculate solar modulation.

The parameters of the primary sources such as the spectral indices γ_i and the break rigidities ρ_i shown in Tab. S-1 are also taken from `HelMod` group [60], which are turned to produced AMS-02 [61] and Voyager 1 [62] data.

In Fig. S-1, we show the local interstellar (LIS) spectrum of CREs calculated by `GalProp-v54` and the solar modulated flux calculated by `HelMod-v4.2`. The LIS CRE flux at the low energy region below 10 MeV shows a good agreement with the Voyager 1 data. The calculated effects of solar modulation agree well with the AMS-02 data. The spectrum of LIS CRE flux follows a power-law and softens at around 5 GeV from $\sim T^{-1.2}$ to $\sim T^{-3.3}$. At higher energies, where the CR fluxes are not affected by the solar modulation, the results are in good agreement with the most recent measurements of AMS, DAMPE and H.E.S.S..

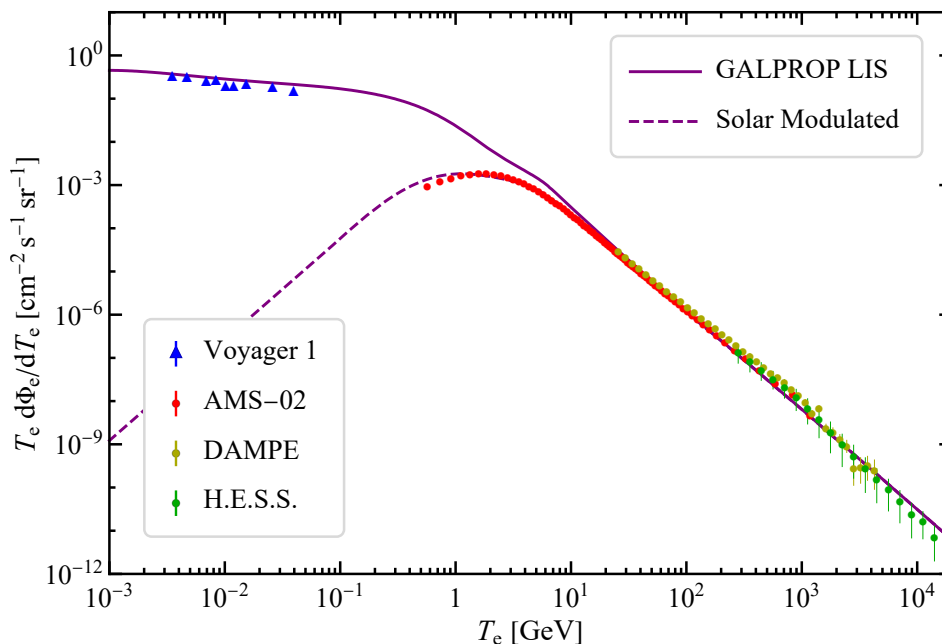


FIG. S-1. CRE flux as a function of kinetic energy calculated by `GalProp-v54` and compared with the data of Voyager 1 [62], AMS-02 [61], DAMPE [89] and H.E.S.S. [90]. The solid line represents the LIS CRE flux and the dashed line stands for that the solar modulated flux calculated by `HelMod-v4.2` [59].

Optimized region of CRDM search at SK

The optimized cone region depends on the morphology of the CRDM flux and experimental backgrounds. In Fig. S-2, we show the signal significance S/\sqrt{B} mentioned in the main text as a function of the cone half-open angle θ , using an isotropic background distribution of $1.96 \text{ kt}^{-1}\text{yr}^{-1}\text{sr}^{-1}$ from the SK MC simulation. The signal is calculated in the energy bin of 0.1–1.33 GeV with detection efficiency included. The maximum is obtained at the region of $\theta \leq 25^\circ$ for $\sigma_{\chi_e} = 2.4 \times 10^{-33} \text{ cm}^2$ at DM particle mass $m_\chi = 1 \text{ MeV}$.

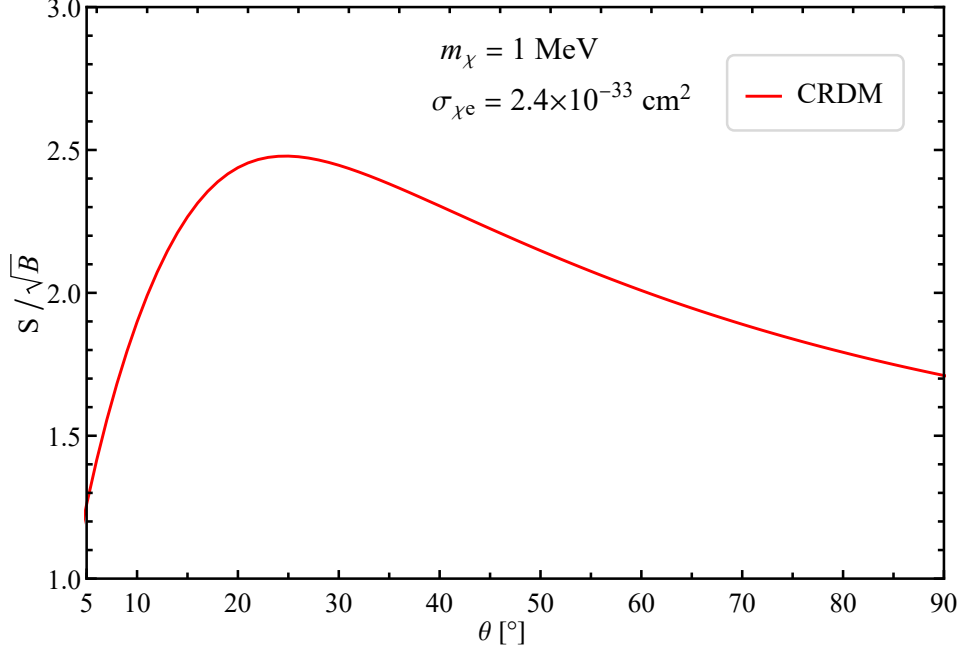


FIG. S-2. The ratio S/\sqrt{B} as a function of polar angle θ with DM mass and cross section taken as $m_\chi = 1$ MeV and 2.4×10^{-33} cm², respectively.

Coefficient of Spherical Harmonics

In this section, we show a more complete set of values for the spherical harmonic expansion coefficients discussed in the main text. We consider two DM density profiles, NFW profile and Einasto profile. The NFW profile is given in the main text. The Einasto profile is parameterised as [47]

$$\rho_\chi^{\text{EIN}}(r) = \rho_\chi^{\text{loc}} \exp \left[- \left(\frac{2}{\alpha} \right) \left(\frac{r^\alpha - R_\odot^\alpha}{r_s^\alpha} \right) \right], \quad (\text{S-5})$$

where $\rho_\chi^{\text{loc}} = 0.42$ GeV cm⁻³ is the local DM intensity in the solar system, $R_\odot = 8.5$ kpc is the distance from solar the the GC, $r_s = 20$ kpc and $\alpha = 0.17$. In Tab. S-2, we show the normalized coefficients $\tilde{a}_{l,m} = |a_{l,m}|/|a_{0,0}|$ for NFW and Einasto profile. The difference between the two profiles is quite small and typically within $\sim 10\%$.

		$\tilde{a}_{1,0}$	$\tilde{a}_{2,0}$	$\tilde{a}_{3,0}$	$\tilde{a}_{4,0}$	$\tilde{a}_{5,0}$	$\tilde{a}_{2,2}$	$\tilde{a}_{3,2}$	$\tilde{a}_{4,2}$	$\tilde{a}_{4,4}$	$\tilde{a}_{5,2}$	$\tilde{a}_{5,4}$
NFW	CRDM	1.00	0.90	0.77	0.63	0.52	0.12	0.12	0.11	0.02	0.09	0.02
	BDM ($n = 1$)	0.63	0.37	0.24	0.17	0.13	0	0	0	0	0	0
	BDM ($n = 2$)	1.28	1.33	1.32	1.29	1.27	0	0	0	0	0	0
Einasto	CRDM	1.06	1.00	0.88	0.75	0.64	0.11	0.11	0.10	0.02	0.09	0.02
	BDM ($n = 1$)	0.68	0.43	0.30	0.22	0.17	0	0	0	0	0	0
	BDM ($n = 2$)	1.36	1.46	1.47	1.45	1.42	0	0	0	0	0	0

TAB. S-2. The extracted normalized coefficients $\tilde{a}_{l,m}$ with $l \leq 5$ for NFW and Einasto profile. The DM mass and cross section are fixed at $m_\chi = 1$ MeV and 10^{-33} cm², respectively.